Very low temperature calorimetry

Unai Urdíroz Urricelqui

Trabajo fin de Máster en Física y Tecnologías Físicas
Departamento de Física de la Materia Condensada

Facultad de Ciencias - Universida de Zaragoza

Curso 2013/2014

Director: Fernando Bartolomé

Instituto de Ciencia de Materiales de Aragón - CSIC

Contents

1 Brief introduction and motivation

1.1 Low temperature heat capacity

The thermal response of a body to applied heat, measured by the specific heat is one of the most important basic parameter of solid state research, providing information about the energy contributions playing a role in the studied system.

The specific heat studies have been closely related to low temperature. As temperature is lowered, the thermal noise that avoids the observation of weak quantum phenomena disappears allowing its study. So that is a key technique to observe quantum phenomena by classical measuremets.

The proposition of the 3rd law of Thermodynamics by Nerst, established that the entropy and thus the specific heat should tend to zero when the absolute zero temperature limit is approached. Einstein and Debye models for the specific heat established the existence of quantum effects at very low temperature that can be related to the energy states of the studied systems. Statistical mechanics allow us to obtain thermodynamic macroscopic parameters of a system such as the heat capacity or entropy, so that these measurements are useful to check theoretical models.

Low temperature calorimetry involve a large number of technical difficulties to deal with, so that, several non-comercial experimental methods have been developed to obtain accurate measurements [1]. All of them have something in common, the use of a heating source that applies a known amount of heat to the sample while its temperature is monitorized.

Both phase transitions, and Schottky anomalies, have a clear fingerprint in heat capacity. Cp(T) is useful in magnetism to obtain energy level configuration [2], in quantum relaxation studies, etc. Calorimeters are also used as radiation and particle detector as an alternative to ionization chamber ones because they do not require efficient charge transport and operate in equilibrium [3]. Their low temperature operation made them the best option in particular applications such as astrophysics, because of their versatility and measurement sensitivity [4].

The aim of this work is the development of a low temperature calorimeter with high magnetic fields using a 9 Tesla coil for the study of magnetic frustrated systems. Besides, the set up may be used to study any kind of temperature and field dependent Cp of any solid system of interest.

1.2 Physical problem: geometrical frustration

In magnets, geometrical frustration prevents the formation of a single-ordered magnetic ground state creating a highly degenerated one [5]. This phenomenon appears when the magnetic ions occupying an ordered lattice are not able to find an absolute energy minimum. This is due to the imposibility to satisfy all contradictory interactions between them. The simplest example is a triangle in which three magnetic moments occupy the corners suffering antiferromagnetic interactions. When the physical conditions acting on the system change (such as: T, H, P or anisotropy), the frustration may be broken and a long-range order (LRO) state could be established.

Frustrated magnets thus lie at the crossroads of two fundamental work fields in condensed matter physics. On the applied side, the instabilities exhibited by frustrated magnets open a window to the richness of nature realized in different materials. On the fundamental side, it is a complex and interesting physical problem to be descrived using different theories [6].

Magnetic materials where lattice symmetries are based on triangles and tetrahedra, such as the pyrochlores or the garnets, may exhibit this phenomenon. In this case, the target of the study will be the Gadollinium Gallium Garnet ($Gd_3Ga_5O_{12}$, GGG) that is very sensitive to the presence of an external magnetic field and has a rich phase diagram [7–11].
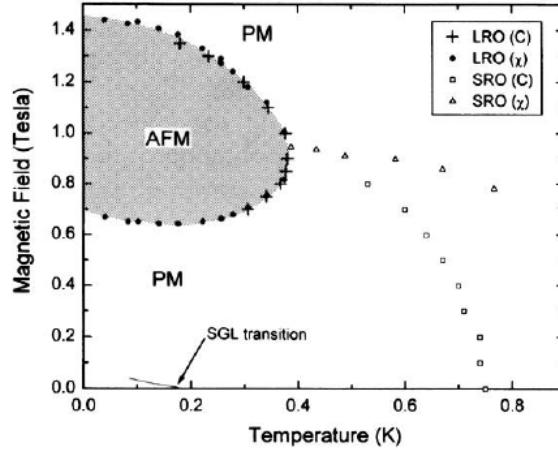

Fig.1: GGG phase diagram depending on temperature and magnetic field based on specific heat and susceptibility measurements.

In this system, the magnetic Gd ions are located at the nodes of two interpenetrating corner-sharing triangle sublattices within the garnet, and the exchanges are almost purely AFM with $\Theta_{Weiss} \sim$ -2 K [12, 13]. The Gd spins are isotropic, although there is a small single ion anisotropy in the GGG of less than 0.04 K. This isotropy leads to the high degree of frustration in GGG which prevents ordering at low fields as observed in isomorphic magnetic garnets such as $Dy_3Ga_5O_{12}$ or other rare earth gallium garnets like $Sm_3Ga_5O_{12}$, $Er_3Ga_5O_{12}$ and $Nd_3G_5O_{12}$ with Néel temperatures below 1 K.

The long term scientific objective is to study the possibility to induce magnetic order in GGG by dilution of a non-isotropic rare earth ion in the Gd site. In particular, we have chosen Eu^{3+}. It differs from other trivalent rare earth ions in having a particular ground state in which there is J=0 while |L|=|S| $\neq$0 and L is aligned antiparallel with S. The introduction of an easy magnetization direction may help to establish the LRO state. It is interesting to check, in case the transition to LRO state appears, if the Eu^{3+} concentration in GGG is higher or lower to the percolation limit. In case the percolation limit is exceeded the studied system changes from GGG with Eu impurities to Gd diluted EuGG. In that case, the conclusions of our study would be totally different.

The stablishment of LRO will be verified by the observation of a clear lambda peak in the heat capacity as a function of external magnetic field applied and temperature. With this data, the phase diagram evolution with Eu impurities would be built.

4

2 Cooling method

2.1 Historical introduction

Temperature is one of the most important thermodynamic variable that can be modified to study the properties of matter and phase transitions. Nowadays, several experimental techniques have been developed to achieve temperatures as low as tens of μK or even effective spin temperatures of nK. These techniques are based on very different experimental effects such as: cryogenic liquids, quanta phenomena or even laser traps.

Low temperature physics have grown since the last decades of the XIX century due to work performed on different laboratories in their race of gas liquefaction: air (N_2+O_2), H_2, and finally He. This last one, was a big temperature jump made by Kamerlingh-Ones in 1908 [14] reaching temperatures below one Kelvin. In 1927 Giauque propose the paramagnetic adiabatic demagnetization [15] allowing to get temperatures of 0.1 K. Finally, in 1962 London, Clarke and Mendoza published a new refrigerator proposal based on the He isotopes mixture properties [16] : the dilution refrigerator.

The main advantages of this refrigeration method is the continuous cooling nature and the availability of using magnetic fields in the experiments. The lowest temperature achieved in these refrigerators has been 2 mK and usually are used as precooling stages for nuclear adiabatic desimanation experiments.

2.2 ^{3}He-^{4}He mixture properties

The cooling power of a dilution refrigerator is based on the physical properties of the ^{3}He -^{4}He mixture [17]. These isotopes have completely different behavior because of their different nuclear spin value. In one hand, ^{4}He has zero nuclear spin obeying the Bose-Einstein statistics, so that, all the atoms can occupy the same energy level. Indeed, it undergoes a phase transition to superfluid state at T=2.18 K where all the atoms are in the ground state. In the other hand, ^{3}He has a half-integer spin value obeying Fermi statistics and Pauli exclusion principle avoiding the presence of two identical atoms in the same energy level. A key fact is that the ^{3}He and ^{4}He are miscible with a rich phase diagram.
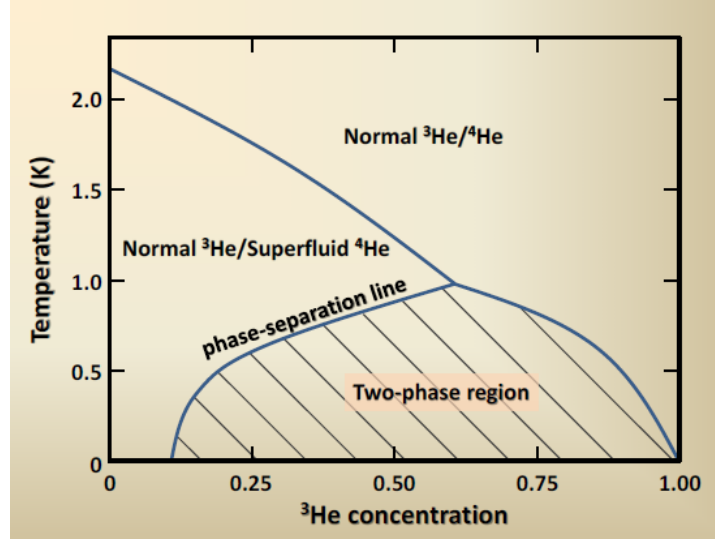
Fig.2: He isotopes mixture phase diagram depending on temperature and the ³He molar fraction

$$x = \frac{n3}{n3 + n4}$$

In the phase diagram, the temperature of the superfluid phase transition of ⁴He (lambda line) decreases with the concentration of ³He in the mixture disappearing in the triple point for x=67.5 and 0.876 K. Cooling the mixture below this point, a separation in two different phases appears: one rich in ⁴He and the other in ³He. Due to its lower density, the ³He rich phase floats on top of the other becoming pure ³He phase when zero temperature is approaching. However, in the ⁴He rich phase, the ³He does not disappear but rather reaches a constant concentration of 6.6%.

The reason for x not been zero at T=0 is, obviously that the binding energy of an ³He atom is bigger in ⁴He liquid than in ³He liquid. In the same way that a liquid ³He needs heat contribution in order to evaporate, the ³He atom absorbs heat from the surroundings, the so called mixture enthalpy, when it changes from the concentred to the diluted phase. So that, the cooling down process is obtained forcing this transitions pumping ³He atoms from the diluted phase. The cooling power, is proportional to the ³He flux trough the main circuit:

$$\dot{Q} = \dot{n}_3 \left[H_d(T) - H_c(T) \right]$$

2.3   Dilution refrigerator

An Oxford Instruments MX40 dilution refrigerator has been used with: base temperature 27 mK, 80 μW cooling power at 100mK, 66 liters of total volume dewar and the possibility of applying magnetic fields up to 9T. The mixture volume is 58 l at 1atm and room temperature with ³He partial volume of 7 l [18]. The different parts involved in the mixture handling procedure are: insert, ⁴He rotary pump,³He pump, gas cabinet, N₂ traps and He trap.
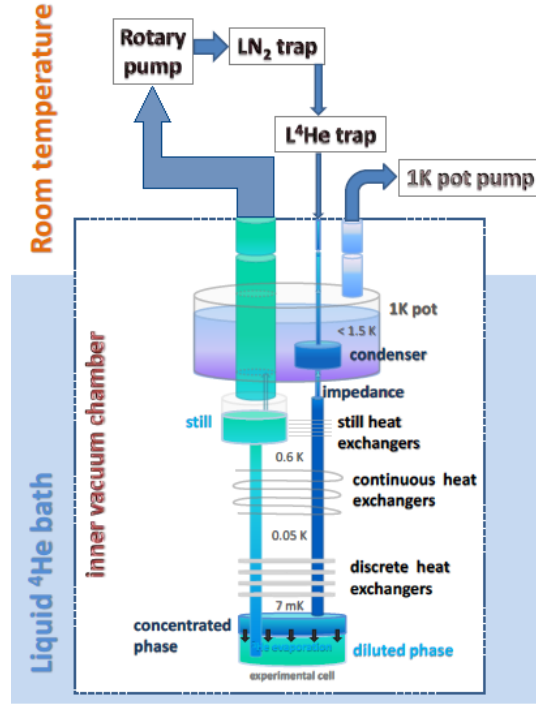
Fig.3: Schematic description of dilution refrigerator [19]. Inner vacuum chamber delimits the inset space inmersed in liquid ^{4}He bath. Arrows indicate ^{3}He flow through the system.

The cooling process could be described as a down-stairs road to the base temperature. In the first step, the system is cooled down to 90 K with liquid Nitrogen. After that, is filled up with liquid Helium taking it down to 4.2 K. Helium is pumped to obtain the working temperature of the 1 K Pot. After this, the ^{3}He -^{4}He mixture is condensed and circulated. Then the system achieves its base temperature.

In the main system circuit, the ^{3}He is pumped from the poor phase in the mixing chamber. It rises exchanging heat with the incoming one in the different stages. Before going back to the mixing chamber, it must pass through the N_2 and He traps and cool down in the heat exchangers. The still must have a vapour pressure fixed in order to maintain an efficient ^{3}He flux [17, 18]. There is a secondary circuit in which the ^{4}He pump takes it from the 1 K Pot to have a fixed cold point.

The whole procedure must be performed maintaining a high vacuum enclosure, and a very clean and leak-free ^{3}He circuit through valvues, pumps and meter-long tubes. All this make the cooling down procedure a slow and rather expensive one.

3   Low temperature thermometry

A very important point in low temperature physics and particularly in calorimetry, is thermometry. In order to measure accurately temperature, we need to have a good thermal contact of the sample with a thermometer: a device whose dependence of a given physical magnitude with temperature is well known. In our case, the resistance thermometry is used since is the best choice at temperatures from 50 mK to 1 K [1,17]. From the two main options,

Germanium and RuO_2, the second one is selected due to its low changes with magnetic fields.

To obtain the best possible measurements, the 4-wire configuration is used in order to eliminate the error caused by resistance of the wires. To measure resistances accurately at very low temperatures, a bridge resistance must be used to apply very low currents, to avoid the self-heating. In this case, a Picowat AVS 47 bridge is used with its analogic exit connected to the input of a HP 3458A multimeter with 8.5 digits to improve the reading resolution.

Temperature measurement is the main source of error in calorimetry measurements. Three main problems have to be considered: the multimeter integation time for each reading, thermometer self-heating and changes in R due to magnetic field(magnetoresistance) [20–23]. Several studies of stability with different excitations and integration times help to choose the best measurement conditions in order to minimize the noise and improve accuracy. In the other hand, magnetic field sweeps at different temperatures will give information about the magnetoresistance of the thermometer and its thermal dependence.

3.1 Thermometers calibration

A Lakeshore full-precision calibrated 2.21 KΩ RuO_2 thermometer is available to be used by the calorimetric set up. It is covered by a brass case holding the RuO_2 chip within a low ^{3}He gas pressure for thermalization but makes it very heavy (3g). This leads to a big thermometer contribution to the measured specific heat.

A calibration experiment has been performed with three thermometers: the calibrated one used as reference and other two RuO_2 chips (of 1.75 KΩ and 2.21 KΩ at RT) with masses of 11 mg. The objective is to have three full calibrated thermometers that could be used on the experiments. The chips have a heat capacity contribution 2 orders of magnitude lower, improving the accuracy in future measurements. Due to unclear reasons, the thermometer holder did not cooled down below 150 mK in this experiments.

RuO_2 resistors are metal-ceramic composites, consisting of a mixture of conductive RuO_2 and Bi_2RuO_2 embedded in a lead silicate glass matrix, deposited on an alumina substrate. For thermal contact, they must be glued to clean surfaces with epoxy or GE Varnish. Their resistance as a function of temperature R(T), can be well fitted by the empirical equation [17]:

$$ln(T) = \frac{1}{\Sigma_i A_i ln \left(R - R_0\right)^i} \text{ with } 0 \leq i \leq 3$$

As it is shown in Fig.5 there is a good quality fitting with errors of 3%-7% between the calculated and the measured temperature for both thermometers.

3.2 Integration time

Integration time is the period of time that the HP multimeter measures the input signal in the multimeter. This value determines the measurement frequency, accuracy, maximum digits of resolution and the noise automatic rejection. With longer integration times, the measurement resolution and accuracy increase, but measurement speed decreases. This parameter will be controlled by the Number of Power Line Cycles (NPLC) selected. The multimeter multiplies
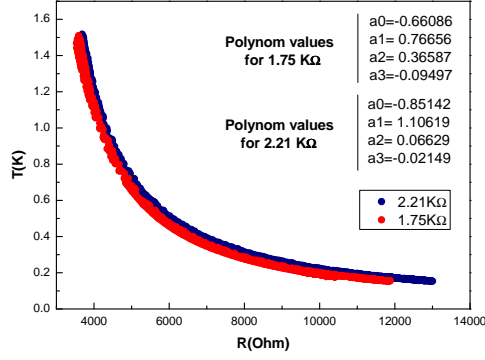
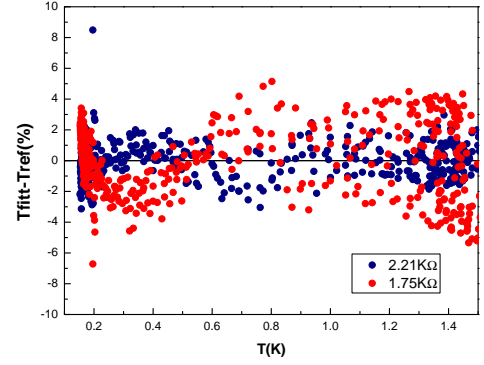**Fig.4**: T(R) curves of the 2.21 KΩ and 1.75 KΩ thermometers taking as reference the calibrated one.

Fig.5: Differences between fitting obtained temperature and measured in percentage.

the specified number of PLCs by its reading period to determine the integration time [24].

In order to determinate the best **integration time** to minimize noise at different temperature ranges, the resistance has been measured with the same excitation but changing the NPLC of the multimeter. Noise windows will be compared in order to get the ideal NPLC.
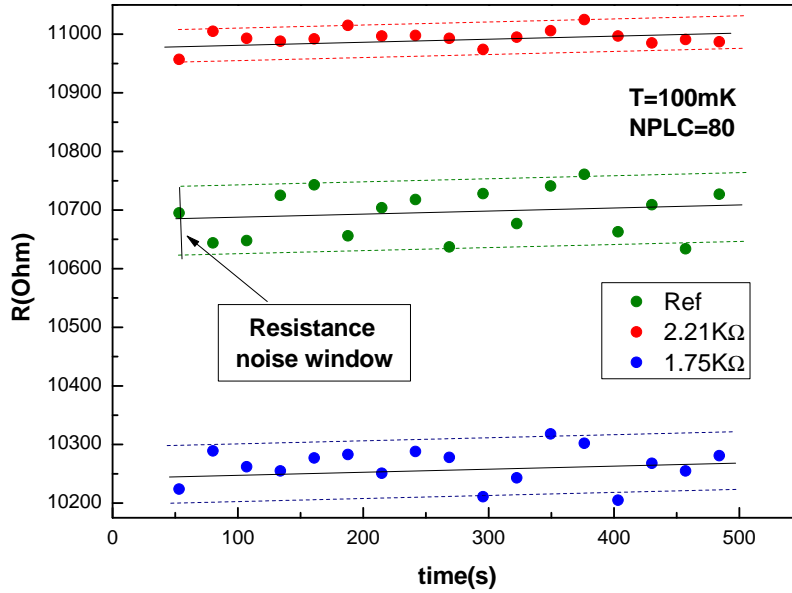

Fig.6: Resistances measured at 150 mK with an excitation lecture of 3 μV and an integration time of NPLC=80(Number of Power Line Cycles).

9

T (mK)	NPLC	Noise (%)
150	20	2.4
150	40	2.0
150	60	1.8
150	80	1.2
400	30	0.5
400	70	0.3
400	100	0.25
500	20	0.17
500	50	0.1

Table1: Noise witdth at different temperatures in function of the selected NPLC.

As temperature is rising, the changes in the noise witdth become lower. So that, it would be interesting to use low NPLC values in order to have more readings. Oppositely, at low temperatures the change is clear and high NPLC values must be selected to minimize the thermal noise. Of course, in the final decision care must be taken to have an integration time significantly lower than the time interval between two temperature readings.

3.3   Reading excitation

The excitation voltage of the AC resistance bridge must be selected to have the best accuracy while avoiding self-heating of the thermometer. Joule dissipation in the sensor causes a rise in its temperature above that of its enviroment. Any difference between the sensor temperature and its surrounding produces a measurement error. To minimize this source of error, requires to find a compromise between the improvement of the signal to noise ratio by using larger excitations and avoiding the self-heating of the sensor.

The calibration report of the reference thermometer indicates that the excitations used were lower than 20 μV below 100 mK and about 60 μV from 100 mK to 1 K.
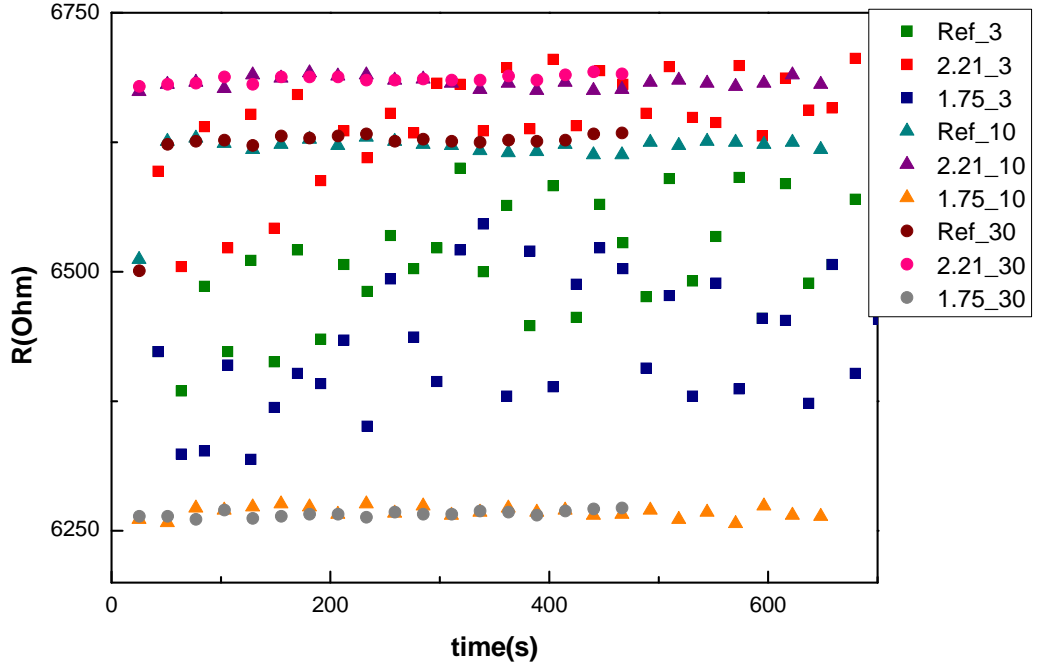
Fig.7: Resistance measurements at 400 mK with different excitation in each case but the same integration time.

At 400 mK, the readings with a 3 μV excitation have a noise error of a 3% in R and 2% in T. This noise fall as the excitation rises to a 0.5% in R and T for 10μV and to a 0.1% in R and T for 30μV. The 1.75 KΩ data for 10 μV and 30 μV have a decrease of a 4% of the value in R that could be due to a self-heating problem. However, this hypothesis does not match with the fact that the value is the same for both excitations. According to the Joule´s law, the heating power for 30 μV would be 9 times bigger than the 10 μV one. In this case, no change is apreciable so that the self-heating is discarded. The same study has been performed also at 150 mK, 500 mK and 700 mK. Considering the obtained results, 30 μV excitations will be used for temperatures higher than 150 mK and 10 μV below .

3.4   Magnetoresistance

Finally, the magnetoresistance [21] has been studied at different temperatures to characterize this effect. Several previous studies have investigated the magnetoresistance of the RuO$_2$ thermometers [25–34] but the results do not always agree and they seem to depend somewhat on the batch.
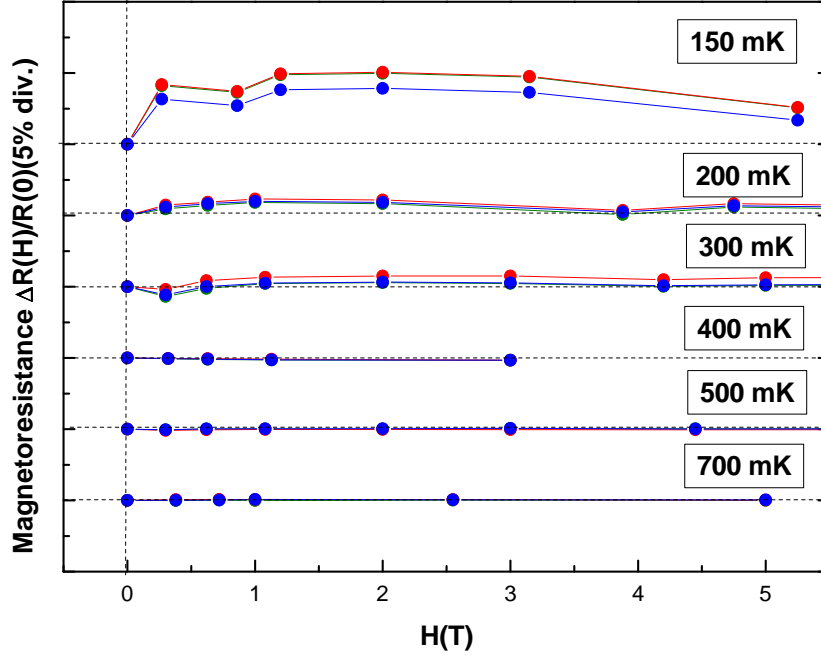
11

Fig.8: Magnetoresistance measurements for different temperatures. The dash line is the x axis for each temperature. In the y axis, the minor ticks represent a 5% and the major ones a 10%. Data in green: reference temperature; red: 2.21 KΩ and blue: 1.75 KΩ.

It the experimental data, it is clear that the magnetoresistance becomes lower as temperature increases. In fact its value is lower than a 0.3% above 300 mK. At this point, a clear hump shape appears with a maximum at fields round to 1 T. This maximum grows as temperature decreases from a 1% at 300 mK to a 9% at 150 mK.

Some results reported on bibliography [1, 17] show that the magnetoresistance response is reproducible only after 60 thermal cycles. As it is shown in Fig.8, the three different thermometers have the same response. Also, some temperatures have been measured more than once with coincident results. This response depends hardly on each thermometer and has no stablished response. Also it seems that in this case, the number of thermal cycles has no influence.

4   Calorimetric methods

Depending on the temperature range and the sample mass available several calorimetric methods may be used in the set up, having in common the temperature monitorization and the heat application. Two of them have been used in this work: quasiadiabatic and relaxation methods.

4.1 Quasiadiabatic method

4.1.1 Theory

The simplest method is the adiabatic or Nerst method where the specific heat definition is applied directly. The temperature increase produced by a known amount of heat applied to the system is measured. In principle, it is applicable when the calorimetric cell is thermally isolated from the thermal reservoir (mixing chamber).

$$Cp = \frac{1}{m} \lim_{\Delta T \to 0} \frac{\Delta Q}{\Delta T}$$

Actually, adiabatic condictions are very difficult to achieve. The so called adiabatic calorimeters are complex and bulky, therefore the adiabatic method is hardly adapted to the space available in dilution refrigerators. A quasi-adiabatic method, in which the sample temperature is allowed to drift slightly due to small thermal leaks has been used [35]. In a quasi-adiabatic calorimeter, the temperature drifts before and after the injection onto the calorimetric setup of a known amount of heat ΔQ are taken as a reference, and used to obtain the subsequent temperature jump ΔT.

In any method, the heat capacity of the total calorimetric setup (sample and addenda) is measured. The addenda contribution, including heater, thermometer, holder and some grease to improve thermal contact shiuld be experimentally determined by means of an "empty cell" measurement, i.e. run with no sample.

This method allows an easy calorimeter design but requires a large sample mass and it is very slow. Measurements are performed step by step increasing the temperature from the base one.
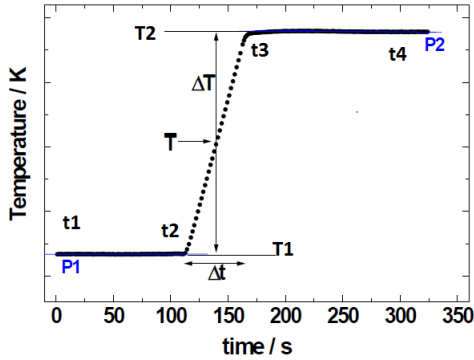

Fig.9: Adiabatic experimental point example measuring temperature in function of time extracted from [36].

Fig.10: Quasiadiabatic calorimeter developed in the Low temperature laboratory.

4.1.2 Experimental setup

A long stick connects the mixing chamber stage with the center of the magnetic coil, a 10 mm diameter spherical volume in which the applied magnetic field has its nominal value and the radial homogeneity better than 99.9%. The stick and the calorimeter are made of oxygen-free high thermal conductivity copper (OFHC) due to its low specific heat (Cp$\approx 1.5 \cdot 10^{-5}$ J/gK

at 0.1 K)and high thermal conductivity (κ_{th}=10 W/cmK at 0.1 K). After the copper stick, a Celotex isolation stage is placed. A brass thermal link is disposed connecting the stick and the calorimetric cell to have relaxation times of $\sim$ 120 s. Finally cilindrical figuration calorimeter (Fig.9) with space for a thermometer and the sample is disposed. In the opposite face of the bottom cover, evanohm* wire is antiiductively winded to be used as heater R=107.76 Ω at RT.

A Picowatt AVS 47 resistance bridge is used to measure temperatures. A Kethley 220PCS current source and a Kethley 2000 multimeter serve as power source and voltimeter respectively. Multimeter measures the voltage in the heater to have an accurate value of the resistance. The source applies the desired current to the heater. All the operation procedure is monitorized from a computer with LabView software.
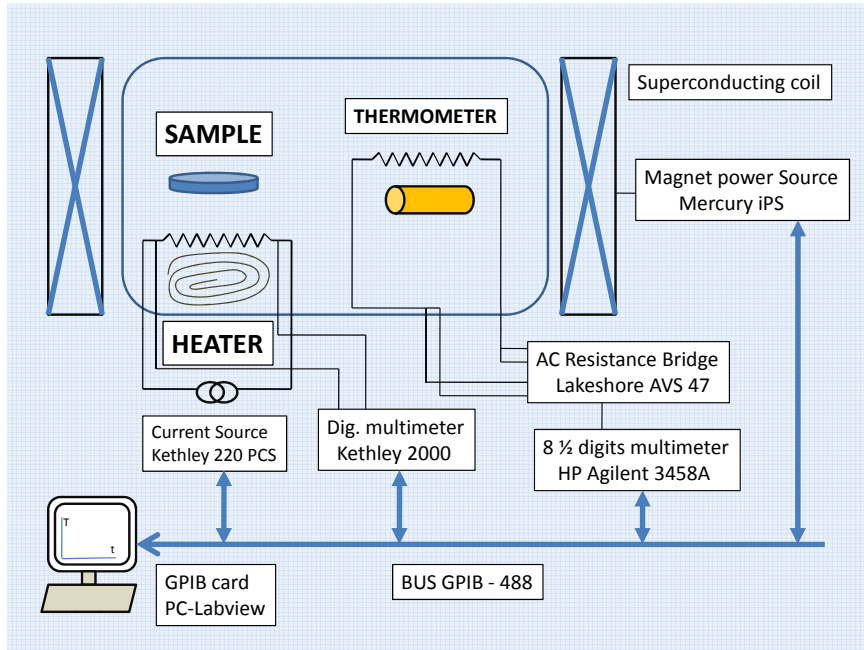

Fig.11: Block diagram of the setup electronic components.

4.2   Relaxation method

4.2.1   Theory

The difficulties to get a large sample mass (of the order of 1 g) and to cool down the system maintaining the adiabatic condition of the calorimetric cell make big mass amount and maintain adiabatic conditions, gave rise to other techniques. The relaxation method is much faster, but the calorimetric cell design and development is more complicated. A proportional-integral-derivative (PID) temperature controller is needed to control the temperature of a thermal reservoir between the mixing chamber and the sample stage.

(*)A Ni(73%), Cr(20%), Al (2.5%), Cu (2%) and Si, Mn (1%) with constant resistance at very low temperatures.
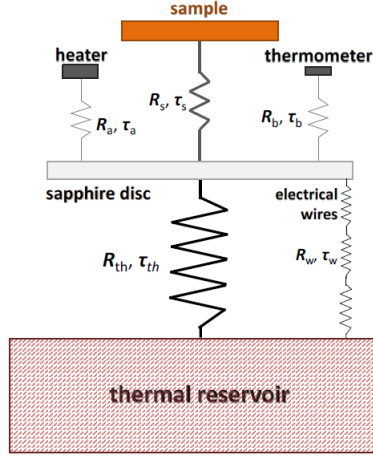
Fig.12: Thermal resistance distribution in the calorimeter. Thermometer and heater -in the copper ring to which sapphire disc is attached to- are considered as part of thermal reservoir.

Thermal resistances in the calorimeter appears as the result of contact boundaries. Also internal resistance in the sample has to be considered. This, must be minimized using high surface-volume ratio in the samples. All the thermal resistances translate into relaxation times, which must satisfy some conditions to have an accurate heat capacity value. In Fig.12, a schematic representation of the most important resistances is shown. The calorimeter relaxation must be dominated by the reservoir- (sample + substrate + sensor) thermal connection. This means that the other resistances must be much smaller $\tau_a \approx \tau_s \approx \tau_b \ll \tau_{th}$. Another requirement is that τ_{th} must be much smaller than the experimental time scale $\tau_{th} \ll \tau_{exp}$. With these considerations, the heating and relaxation temperature curves obey the equations:

$$\Delta T(t) = \frac{P}{K_H} \left(1 - \exp^{-t/\tau} \right)$$

$$T(t) = T_0(t) + \Delta T_\infty \exp^{-t/\tau}$$

A thermal link is established between the reservoir and the sapphire platelet to have relaxation times needed to find a compromise between maintaining a relatively fast measurement (between 1 and 5 minutes per point) and having a detailed determination of the exponential temperature vs. time growth and decay.

Two alternative methods can be consider: the standard and the fast one (Fig.13). In the first part of the standard, the heating power is switched on until the steady-state equilibrium between the heating and the cooling power is achieved. At this point, the temperature increase becames constant $\Delta T_\infty = P/K_H$. From a exponential fitting of the decay curve, the relaxation time is obtained. Knowing the thermal conductance from the heating curve, the specific heat will be obtained: $C_p = K_H \cdot \tau$.

However, when the relaxation time grows, usually with temperature, the experimental errors become bigger due to the changes in the base line. In this case, the so called "fast relaxation method" is a better choice. It is not necessary to wait for the full stabilization of the calorimetric setup at the equilibrium, and heating can be fitted to an exponential curve. Then the heat pulse can be switched off and fitting the relaxation to another exponential curve

Cp determination starts. This procedure can be repeated at will to reduce the uncertainty of the measurement.
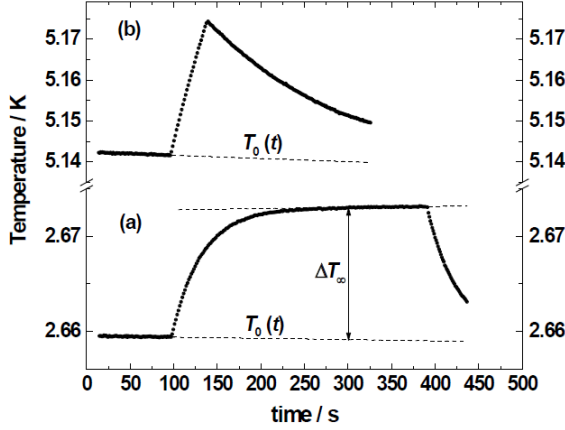

Fig.13: Experimental points obtained using the normal relaxation method(a) and the alternative fast one (b) extracted from [36].

Fig.14: Isoperibol calorimeter brought from Kamerlingh Onnes Laboratorium of the University of Leiden, used as example in the development of our own. Some parts have been used in our model.

4.2.2 Data treatment

The procedure starts with the linear fitting of the exponential relaxation decay in a semi-log plot (Fig.15) obtainig the time constant τ. As τ is known, a simple variable change is done, t$\rightarrow \delta = [1 - exp(-t/\tau)]$, turning the heating curve into $\Delta T(\delta) = (P/K_H)\delta$. Thus, a simple least-square linear fit provides the missing parameter K_H, and heat capacity is obtained again from $Cp = K_H \cdot \tau$ (Fig.16).

However, in real systems the thermal resistance between the sample and the holder do not satisfy $\tau_s \ll \tau_{th}$. So that relaxation curves show two different contributions: the first and the fast one, related to the relaxation of the sample with the calorimeter cell; and the second one, the relaxation of the whole system with the surrondings.

In fact, the Quantum Design Physical Properties Measurement System (PPMS) uses its own theoretical "two τ" model [37]. In this model, two main pre-measurement studies must be done in order to obtain an accurated specific heat value: empty calorimeter and thermal conductance of the link as a function of temperature and external field is necesary. Also is important to consider that this first contribution usually is almost negligible in the PPMS because the cell and mass amount are selected to optimize the measurement. In our case, relaxation measures have been made with large sample mass that avoid the optimization. Dr. Ana Arauzo from the SMF (Servicio de Medidas Físicas) confirmed that contribution in our case was much larger than in PPMS cases due probably to the large sample mass and surface-volume ratio in the sample pill.

Empty calorimeter and thermal link response have not been measured. Copper and Apiezon N heat capacity are known [17] so that despite not having an empty calorimeter
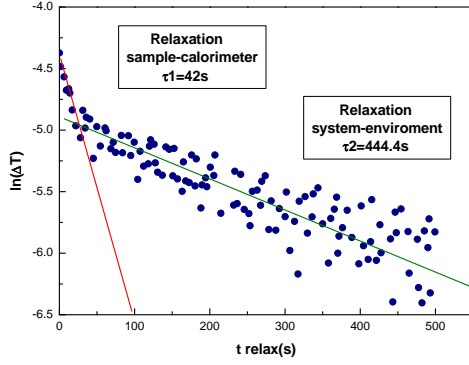
16

Fig.15: Experimental points on a semi-logarithmic representation of the system relaxation. Linear fitting have been made to obtain time constant.
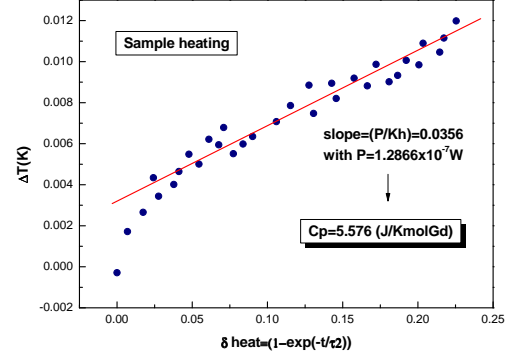

Fig.16: Linear fitting of heating points gave thermal conductance with which the specific heat is obtained.

measurement, a rough Cp estimation has been done using: $Cp = m_{co}(\gamma_{co} \cdot T + A_{co} \cdot T^3) + m_{Apiez}(A_{Apiez} \cdot T^3)$ with 12 g of copper and 8.6 mg of Apiezon N. In the other hand, the thermal link response is unknown. The obtained values from data treatment are supported on an approach neglecting the first fast relaxation.

4.2.3 Experimental setup

Several calorimeteres are reported in literature [38–41]. In our case (Fig.17), the calorimetric holder is a 12mm sapphire platelet mechanically attached to the thermal reservoir by kapton strips. Thermal reservoir is made of OFHC copper. The sapphire is used due to its low Cp (Cp≈ 0.1 nJ/gK at 0.1 K), good thermal conductivity ($\kappa_{th} \approx 20\mu W/cmK$ at 0.1 K) and mechanical strength. Sample holder is connected to the mixing chamber stage with the same stick-isolator-thermal link configuration as in the previous design. To control the reservoir temperature via PID, Evanohm wire heater and full calibrated thermometer are disposed. In the sapphire holder a chip thermometer is placed and a thin film is deposited to be the heater with R=259.95Ω at RT.
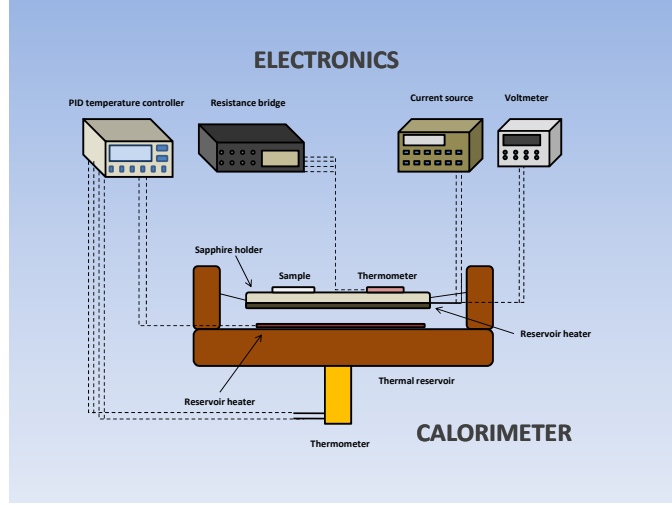
Fig.17: Schematic description of the isoperibol calorimeter control with electronic equipment. Dashed lines, correspond to RT electrical wiring.

The electronic components used in this case are the same the PID temperature controller introduction to monitorize the thermal reservoir.

5   Measurements

First measurements have been performed in a GGG pure sample of 97 obtaining in total 20 Cp points. As the most interesting contribution in the GGG heat capacity is the magnetic one related to the Gd^{3+} ions, the obtained data are exposed in units of J/K per Gd mol.

Zero field measurements at 270 mK, 300 mK and 320 mK are shown in the Fig.18 where are compared with Schieffer data [7] and PPMS obtained data. Then temperature has been stabilized at 130 mK to measure Cp as a function of externeal the field from 0.2 T to 2 T with a higher point density near the phase transition. The same was done at 320 mK with fields from 0 T to 1.8 T. This points are shown as Cp(H) curves at a fixed T in Fig.20 in comparison again with Scieffer data [7]. Finally experimental points for 0.65 T, 0.7 T and 0.75 T at temperatures from 87 mK to 345 mK are compared with Schieffer [7] and Tsui [11] data in Fig.19.
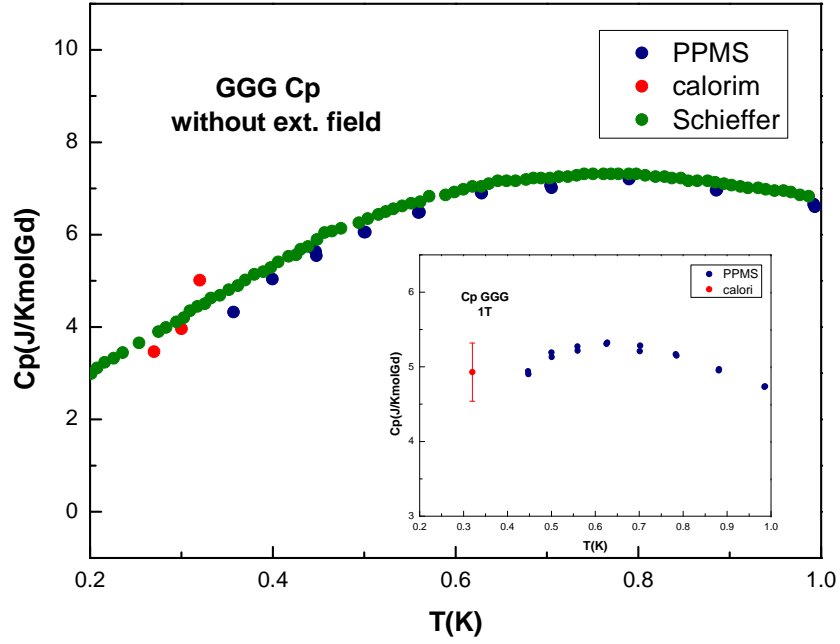
Fig.18: Specific heat measurements at zero field with handmade calorimeter compared with the exposed by Schieffer on [7] and with other values obtained using PPMS. **Inset**: Experimental point for H=1T in comparison with PPMS data.

In Fig.18, the differences with Schieffer data go from a 10% to a 15% within the error bar that in this case reach a 30% in the three points due to the noisy data curves. In the inset, the point measured for 1 T field applied has an error of a 25% respect to the PPMS data curve out of its 9% error bar.
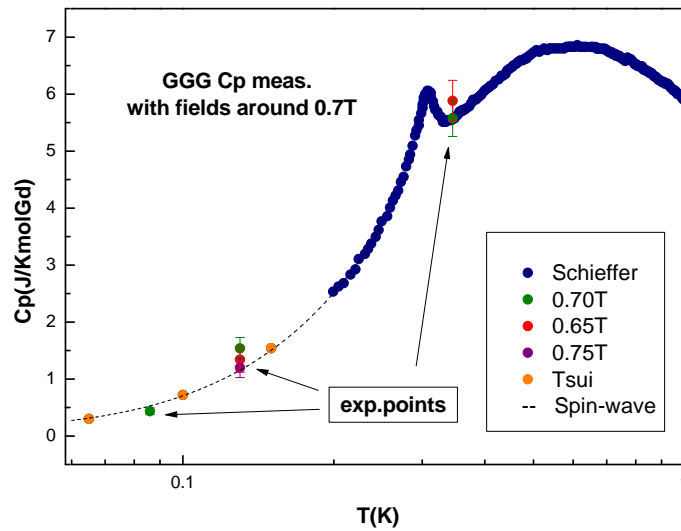

Fig.19: Experimental values at fields of 0.65T. 0.7T and 0.75T compared with the exposed on [11].

Figure 19 is a compilation of the measurements performed near the phase transitio at fields around 0.7 T. A fit of the Schieffer and Tsui [7] [11] low temperature specific heat to a curve $C \propto T^{3/2}$ corresponding to the contribution of the antiferromagnetic spin waves on the ordered phase is considered as reference to compare with experimental points. All the points agree with literature with differences respect to the $T^{3/2}$ fit within the error bars.
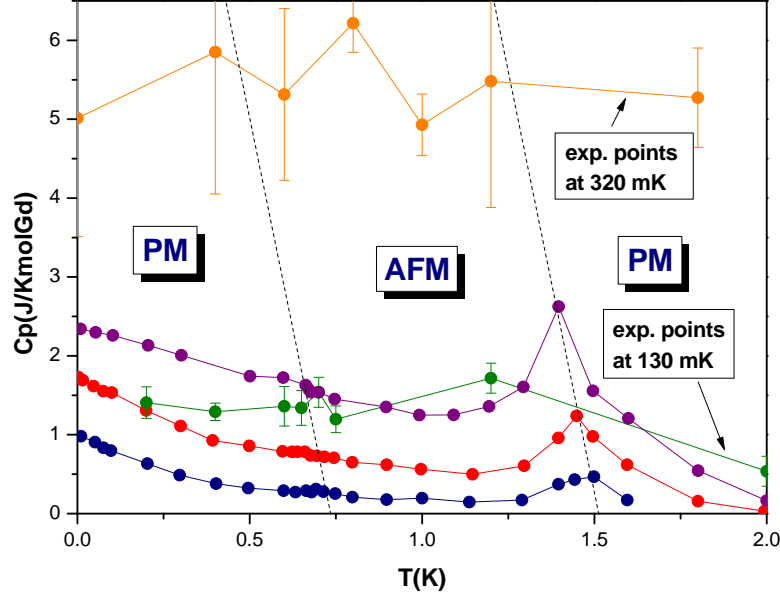

Fig.20: GGG specific heat as a function of the applied field at several low temperatures. From the bottom to the top in temperature increase order: 65 mK (blue), 100 mK(Schieffer)(red), 130 mK(exp.) (green), 150 mK(Schieffer)(purlple) and 320 mK(exp.)(yellow).

Finally in Fig.20 Cp(H) is shown at different temperatures to observe magnetic phase transitions. Observing the GGG phase diagram (Fig.1) [7] is clear that two different phase transitions should be observed at the exposed temperatures. According to Tsui data, it seems that the phase transition that occurs at fields around 0.7 T is less abrupt than the one at field around 1.4 T.

The experimental data for 130 mK has a qualitative agreement with Tsui Cp(H) curves [11] with error bars of a 15%. Furthermore, the phase transition at 0.7 T is observed. However at 320 mK, there are not enough measured points to observe neither of the phase transitions. Also, the error achieves values of a 30% because of the noisy data curves again.

5.1 Experimental conclusions

A normal calorimeter has been designed, developed and proved. The sample mass and the calorimeter used in the experiment were optimized to measure using the quasiadiabatic method. However, relaxation measurements were performed due to the setup response. Although the experimental setup was not appropriate to use the relaxation method, 20 experimental points were obtained in agreement with literature [**?**, 7] and errors up to a 30% in

the worse fittings.

To optimize the experimental setup for relaxation method an isoperibol calorimeter is being developed. Besides the cell contribution is minimum, the sample mass decrease critically as it does the first relaxation improving measurement accuracy. Nowadays the isoperibol calorimeter is in mounting process.

6   Conclusions

This work is the starting point of a very low temperature calorimetric measurement system development with applied magnetic fields. An important effort has been done to get into low temperature physics. Also, the complete experimental setup building has been done, from the design to the mechanical assembly.

a) Dilution refrigerator operation processes have been studied. Now a complete cooling down procedure can be completed without any help.

b) Three thermometer complete calibration has been done to obtain future accurate temperature measurements. Self-heating, integration time noise and magnetoresistance have been studied and characterized.

c) A normal calorimetric cell and measurement software have been built and used on a first attempt of quasiadabatic measure. An isoperibol calorimeter and relaxation software are being developed.

d) Some experimental points are obtained using an approach. The error go from a 5 to a 30% in the worst fittings but are in a qualitative agreement with literature. A phase transition peaks is observed at 130 mK and 0.7 T.

References

[1] G. Ventura and L. Risegari, *The art of cryogenics: low-temperature experimental techniques.* Elsevier, 2010.

[2] F. L. Villalta, *Estudio experimental del efecto tunel cuántico en materiales magnéticos.* PhD thesis, ICMA-Universidad de Zaragoza, 1997.

[3] M. P. Borderías, *Low temperature calorimetry applications: radiation detectors and material characterization.* PhD thesis, ICMA-Universidad de Zaragoza, 2011.

[4] G. Stewart, "Measurement of low-temperature specific heat," *Review of Scientific Instruments*, vol. 54, no. 1, pp. 1–11, 1983.

[5] R. M. . A. Ramírez, "Geometrical frustration," *Physics today*, 2006.

[6] L. Balents, "Spin liquids in frustrated magnets," *Nature*, vol. 464, no. 7286, pp. 199–208, 2010.

[7] P. Schiffer, A. Ramirez, D. Huse, and A. Valentino, "Investigation of the field induced antiferromagnetic phase transition in the frustrated magnet: gadolinium gallium garnet," *Physical review letters*, vol. 73, no. 18, p. 2500, 1994.

[8] O. Petrenko, C. Ritter, M. Yethiraj, and D. M. Paul, "Investigation of the low-temperature spin-liquid behavior of the frustrated magnet gadolinium gallium garnet," *Physical review letters*, vol. 80, no. 20, p. 4570, 1998.

[9] S. Dunsiger, J. Gardner, J. Chakhalian, A. Cornelius, M. Jaime, R. Kiefl, R. Movshovich, W. MacFarlane, R. Miller, J. Sonier, *et al.*, "Low temperature spin dynamics of the geometrically frustrated antiferromagnetic gadollinium gallium garnet," *Physical review letters*, vol. 85, no. 16, p. 3504, 2000.

[10] A. Ramirez and R. Kleiman, "Low-temperature specific heat and thermal expansion in the frustrated garnet gd3ga5o12," *Journal of Applied Physics*, vol. 69, no. 8, pp. 5252–5254, 1991.

[11] Y. Tsui, C. Burns, J. Snyder, and P. Schiffer, "Magnetic field induced transitions from spin glass to liquid to long range order in a 3d geometrically frustrated magnet," *Physical review letters*, vol. 82, no. 17, p. 3532, 1999.

[12] O. Petrenko, D. M. Paul, C. Ritter, T. Zeiske, and M. Yethiraj, "Magnetic frustration and order in gadolinium gallium garnet," *Physica B: Condensed Matter*, vol. 266, no. 1, pp. 41–48, 1999.

[13] W. Kinney and W. Wolf, "Magnetic interactions and short range order in gadolinium gallium garnet," *Journal of Applied Physics*, vol. 50, no. B3, pp. 2115–2117, 2008.

[14] H. Kamerlingh Onnes, "The liquefaction of helium.," *Koninklijke Nederlandse Akademie van Weteschappen Proceedings Series B Physical Sciences*, vol. 11, pp. 168–185, 1908.

[15] W. Giauque, "A thermodynamic treatment of certain magnetic effects. a proposed method of producing temperatures considerably below 1 absolute," *Journal of the American Chemical Society*, vol. 49, no. 8, pp. 1864–1870, 1927.

[16] H. London, G. Clarke, and E. Mendoza, "Osmotic pressure of he 3 in liquid he 4, with proposals for a refrigerator to work below 1 k," *Physical Review*, vol. 128, no. 5, p. 1992, 1962.

[17] F. Pobell, *Matter and methods at low temperatures*, vol. 2. Springer, 1996.

[18] *Oxford Instruments Kelvinox MX40 Dilution Refrigerator Option Manual*.

[19] T. P. Castañeda, *Low-temperature specific heat of hyperaged and ultrastable glasses*. PhD thesis, Universidad Autónoma de Madrid, 2013.

[20] N. Fortune, G. Gossett, L. Peabody, K. Lehe, S. Uji, and H. Aoki, "High magnetic field corrections to resistance thermometers for low temperature calorimetry," *Review of Scientific Instruments*, vol. 71, no. 10, pp. 3825–3830, 2000.

[21] R. Goodrich, D. Hall, E. Palm, and T. Murphy, "Magnetoresistance below 1k and temperature cycling of ruthenium oxide–bismuth ruthenate cryogenic thermometers," *Cryogenics*, vol. 38, no. 2, pp. 221–225, 1998.

[22] A. W. Stadler, "Noise properties of thick-film resistors in extended temperature range," *Microelectronics Reliability*, vol. 51, no. 7, pp. 1264–1270, 2011.

[23] R. Sahul, V. Tasovski, and T. Sudarshan, "Ruthenium oxide cryogenic temperature sensors," *Sensors and Actuators A: Physical*, vol. 125, no. 2, pp. 358–362, 2006.

[24] *HP-3458A Operating Programming and Configuration Manual*.

[25] W. Schoepe, "Conduction mechanism in granular ru02-based thick-film resistors," *Physica B: Condensed Matter*, vol. 165, pp. 299–300, 1990.

[26] A. Briggs, "Characterization of some chip resistors at low temperatures," *Cryogenics*, vol. 31, no. 11, pp. 932–935, 1991.

[27] G. G. Ihas, L. Frederick, and J. McFarland, "Low temperature thermometry in high magnetic fields," *Journal of low temperature physics*, vol. 113, no. 5-6, pp. 963–968, 1998.

[28] M. Watanabe, M. Morishita, and Y. Ootuka, "Magnetoresistance of ruthenium oxide based resistance thermometers below 0.3 k," *Cryogenics*, vol. 41, no. 3, pp. 143–148, 2001.

[29] B. Neppert and P. Esquinazi, "Temperature and magnetic field dependence of thick-film resistor thermometers," *Cryogenics*, vol. 36, no. 4, pp. 231–234, 1996.

[30] K. Uhlig, "Magnetoresistance of thick-film chip resistors at millikelvin temperatures," *Cryogenics*, vol. 35, no. 8, pp. 525–528, 1995.

[31] M. Siqueira, R. Viana, and R. Rapp, "Carbon and thick film chip resistors as thermometers for heat capacity measurements below 1 k," *Cryogenics*, vol. 31, no. 9, pp. 796–800, 1991.

[32] R. Willekers, F. Mathu, H. Meijer, and H. Postma, "Thick film thermometers with predictable r/t characteristics and very low magnetoresistance below 1 k," *Cryogenics*, vol. 30, no. 4, pp. 351–355, 1990.

[33] M. Meisel, G. Stewart, and E. Adams, "Thick film chip resistors as millikelvin thermometers," *Cryogenics*, vol. 29, no. 12, pp. 1168–1169, 1989.

[34] W. Bosch, F. Mathu, H. Meijer, and R. Willekers, "Behaviour of thick film resistors as low temperature thermometers in magnetic fields up to 5 teslas," *Cryogenics*, vol. 26, no. 1, pp. 3–8, 1986.

[35] F. Bartolomé, *Interacciones magnéticas en compuestos de tierra rara y metal de transición*. PhD thesis, ICMA-Universida de Zaragoza, 1995.

[36] E. Pérez-Enciso and M. A. Ramos, "Low-temperature calorimetry on molecular glasses and crystals," *Thermochimica Acta*, vol. 461, no. 1, pp. 50–56, 2007.

[37] *Physical Property Measurement System Heat Capacity Option Manual, Quantum Design Inc.*

[38] R.J.Schutz, "Thermal relaxation calorimetry below 1 k," *Review of Scientific Instruments*, vol. 45, no. 456, 1974.

[39] R. Bachmann, F. DiSalvo Jr, T. Geballe, R. Greene, R. Howard, C. King, H. Kirsch, K. Lee, R. Schwall, H.-U. Thomas, *et al.*, "Heat capacity measurements on small samples at low temperatures," *Review of Scientific Instruments*, vol. 43, no. 2, pp. 205–214, 2003.

[40] H. Wilhelm, T. Luhmann, T. Rus, and F. Steglich, "A compensated heat-pulse calorimeter for low temperatures," *Review of scientific instruments*, vol. 75, no. 8, pp. 2700–2705, 2004.

[41] H. Tsujii, B. Andraka, E. Palm, T. Murphy, and Y. Takano, "Calorimeter for a top-loading dilution refrigerator in high magnetic fields," *Physica B: Condensed Matter*, vol. 329, pp. 1638–1639, 2003.